International Journal of Fluid Power 11 (2010) No. 2 pp. 15-24

SIMULATION OF THE LUBRICATING FILM BETWEEN CONTOURED PISTON AND CYLINDER

Stefan Gels and Hubertus Murrenhoff

Institute for fluid power drives and controls (IFAS) of RWTH Aachen University
Stefan.Gels@ifas.rwth-aachen.de, Hubertus.Murrenhoff@ifas.rwth-aachen.de

Abstract

Axial piston pumps are used in several industrial applications. The geometry of the probably most important interface of these pumps, the piston-cylinder-contact, is mostly optimized by comparing test bench results. Only a few simulation tools have ever been used to optimize the geometry such as gap width, cylinder length, etc.

For the DFG-supported project "Axial piston machines with PVD-coated components" both, piston and cylinder, are to be coated or should consist of hardened material, so that running-in is no longer possible. The contour of piston and cylinder therefore needs to be machined before the parts are used in the axial piston pump. Simulations of different contours as well as gap widths and cylinder lengths are therefore necessary to avoid a large number of test-bench measurements.

In this publication a simulation tool is presented, which allows to vary the geometry and contouring of the moving parts. It is shown that the contouring and geometry can be optimized for specific working points.

Keywords: lubricating film, Reynolds-equation, axial piston machines

1 Introduction

1.1 Investigation of the Lubricating Film between Piston and Cylinder in the Past

Investigations of the lubricating film, especially between piston and cylinder of axial piston machines, have already been carried out by a couple of authors with different conditions and goals.

Renius (1974) was the first one who measured the axial friction forces of the piston-cylinder-contact with his single-piston test-bench.

A helpful theoretical overview of the forces and torques related to the piston-cylinder-contact is given by Ivantysynova (1993). Manring (1999) extends this theoretical overview and verifies simulations with test-bench results.

Liu (2001) presents a multiple body system of a hydrostatic gear, where the hydrodynamic effects were replaced by spring-damper-elements. Later on Deeken (2002) worked with a combined tool of multiple-body-simulation and a network of hydraulic resistors and capacities. Kleist (2002) created a simulation tool and could show the occurrence of mixed friction. He obtained good results which could later be compared with test-bench-results from single-piston test-benches.

Wieczorek (2002) made great progress with his simulation tool CASPAR. He considered three of the four tribological interfaces in axial piston machines and used a non-isothermal model to solve the Reynolds-equation. The average-flow-model by Patir and Cheng (1978) is used as well.

Olems (2001) was able to measure the temperature distribution and compared the results with simulation results from the tool CASPAR.

Using the simulation tool of Wieczorek, Lasaar (2003) firstly investigated contoured pistons. He attached a convex shape over the whole piston length for the simulation and could show improvements concerning leakage and friction forces. He also measured axial and tangential friction forces on a test-bench and could confirm the simulation results.

Later on, Scharf (2005) worked with contoured pistons for low-speed machines, especially axial piston motors.

This manuscript was received on 25 May 2009 and was accepted after revision for publication on 15 June 2010

1.2 Contents of this Publication

Within the technology transfer project "Axial Piston Machines with physical vapor deposition (PVD)-coated Components", which is part of the collaborative research centre (CRC) 442, the sliding parts of the tribological interfaces in an axial piston machine, especially the piston-cylinder-contact, are to be equipped with PVD-coatings or hardened surfaces. The target is to remove the brass and bronze from the machine which causes faster ageing of the used fluid especially when native esters are in use. Moreover PVD-coatings seem to be suitable for use in hydrostatic machines, as described by van Bebber (2003).

The run-in, which is known from cylinders made of brass or bronze, usually yields a reduction of friction forces. This phase takes a couple of hours, during which the over-all efficiency of the axial-piston machines increases. The reason for this behavior is that the soft material of the cylinder is "ground" to a trumpet-like form, which improves the build-up of the lubricating film.

Using a hard-hard-combination for the materials of piston and cylinder, abrasion and therefore running-in is no longer possible. A contouring on both parts and both ends of piston and cylinder has to be machined before the surface coating is applied. An open question is what contour should be used. A good contour might be the run-in contour of the smooth bronze cylinder of ordinary machines, but it is not known, whether there is a better contouring. Moreover, the optimal contour of the piston cannot be taken from a piston after running-in, since the conventional pistons are hardened and do not show abrasion, thus leaving the contouring on the soft cylinder.

Therefore a simulation tool is required to determine good contours and useful combinations of gap width and cylinder length. A systematic simulative investigation was performed and the results are content of the publication at hand. The simulation tool itself is described shortly as well.

2 Description of the Simulation Tool

In contrast to most of the simulation tools described above the one used for this publication was planned to be a fast simulation tool, which could be used on every standard PC. A simulation with 100 time steps for each revolution and a sufficient meshing should take less than 15 minutes to be able to perform parameter variation with the tool.

2.1 Lubricating Film

The simulation tool is basically a solver for the Reynolds equation, as shown in Eq. 1. The variable h is the gap width of the lubricating film, p is the pressure, U and V are the axial and rotational speed of the piston.

$$\frac{\partial}{\partial x}\left(\frac{h^3}{\eta}\cdot\frac{\partial p}{\partial x}\right)+\frac{\partial}{\partial y}\left(\frac{h^3}{\eta}\cdot\frac{\partial p}{\partial y}\right)= 6\left(\frac{\partial(hU)}{\partial x}+\frac{\partial(hV)}{\partial y}+2\frac{dh}{dt}\right) \tag{1}$$

In the simulation tool, the Reynolds equation should be applied on a small but macroscopic element of the lubricating film. In order to apply the Reynolds equation on such an element, each differential quotient is replaced by a difference quotient, as it is exemplary shown in Eq. 2, where A might be any variable or term of the Reynolds equation and *Left* and *Right* are two arbitrary x-positions.

$$\frac{\partial}{\partial x}(A)=\frac{1}{x_{\text{Right}}-x_{\text{Left}}}\left[A_{\text{Right}}-A_{\text{Left}}\right] \tag{2}$$

Using Eq. 2 for "disassembling" the Reynolds equation, Eq. 1 receives the following form. To make it easier to read, only the summands for the x-direction are shown in Eq. 3, while the y-direction is neglected.

$$\frac{1}{x_{\text{Right}}-x_{\text{Left}}}\left[\left(\frac{h^3}{\eta}\cdot\frac{\partial p}{\partial x}\right)_{\text{Right}}-\left(\frac{h^3}{\eta}\cdot\frac{\partial p}{\partial x}\right)_{\text{Left}}\right]= 6\left(\frac{1}{x_{\text{Right}}-x_{\text{Left}}}\left[(hU)_{\text{Right}}-(hU)_{\text{Left}}\right]+2\frac{dh}{dt}\right) \tag{3}$$

The element of the lubricating film, on which the equation should be applied, is shown in Fig. 1. It has the length l and width b. The cylinder, which is represented by the lower plane in Fig. 1, is fixed, while the upper plane, which is part of the piston, can move in x- and y-direction. The distance between the two planes is the variable h which was already used in the Reynolds equation. Oil flow is possible over all 4 borders of the element.

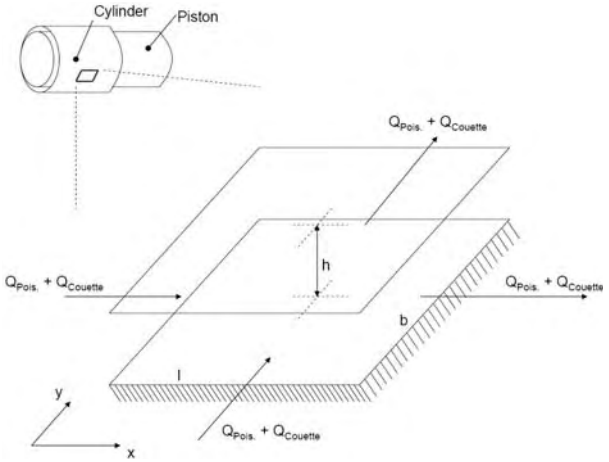

Fig. 1: *Element of the lubricating film*

Rearranging the summands of Eq. 3 and multiplying by $b\cdot l/12$ yields Eq. 4.

$$\frac{1}{l}\left[\left(\frac{bh^3l}{12\eta}\cdot\frac{\partial p}{\partial x}\right)_{\text{Right}}-\left(\frac{bh^3l}{12\eta}\cdot\frac{\partial p}{\partial x}\right)_{\text{Left}}\right] -6\frac{1}{l}\left[\left(\frac{bhUl}{12}\right)_{\text{Right}}-\left(\frac{bhUl}{12}\right)_{\text{Left}}\right]=bl\frac{dh}{dt} \tag{4}$$

This can be written as:

$$Q_{\text{Poiseuille,Left}} + Q_{\text{Couette,Left}} - Q_{\text{Poiseuille,Right}} - Q_{\text{Couette,Right}} = b\, l\, \frac{d\, h}{dt} \tag{5}$$

With:

$$Q_{\text{Poiseuille}} = -\frac{b\, h^3}{12\eta} \cdot \frac{\partial p}{\partial x} \qquad Q_{\text{Couette}} = \frac{b\, h\, U}{2} \tag{6}$$

The flow over one border of the element is depicted in Fig. 2 in a simplified manner.

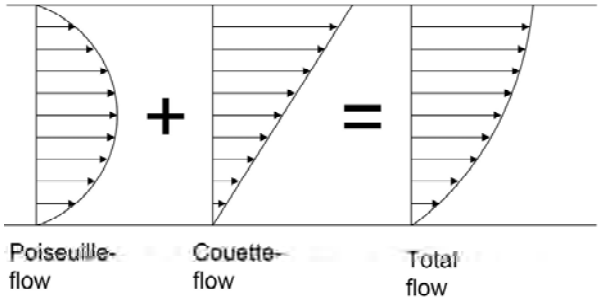

Fig. 2: *Superposition of Poiseuille- and Couette-flow*

The summands for the y-direction have to be added at last. This yields to a flow balance with 8 independent flows over the borders of the considered element and one summand for the changing of the average height of the element. So instead of the Reynolds equation in Eq. 1 the discretised and disassembled equations Eq. 5 and Eq. 6 are implemented in the simulation tool presented here.

The elements are arranged in a quadratic manner, as shown in Fig. 6. The flow balance is computed for each joint of the black grid of the lubricating film, while the Couette- and Poisseuille-flow are computed for each linking line between two joints.

2.2 Theory of Bending Beam

First results with the new simulation tool showed that there is an impact of the bending of the piston on the simulation results. The reason is that the bending of the piston is almost as large as the gap width of the piston and therewith influences the build-up of the lubricating film significantly. Therewith it seems necessary to consider the bending in the simulation tool.

Meshing of the whole piston is one way to take its bending into account. But the simulation time will increase significantly. Another possibility is to use the theory of the bending beam. It is easier to compute and it is accurate enough for a rather simple load situation like the one considered here.

The theory of bending beam, as it is described by Weichert (1999) for example, gives a connection between the acting forces and torques and the bending of the piston. The piston is demounted in several cross sections. An exemplary look at one of these cross sections is shown in Fig. 3.

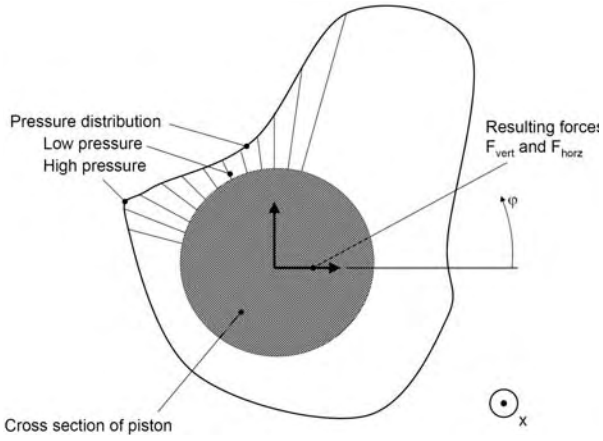

Fig. 3: *Cross section of the piston and acting pressure field*

The grey cross section of the piston in Fig. 3 is surrounded by a pressure field. If the pressure is high, the line for the pressure distribution is next to the cross section. A higher pressure is represented by a higher distance between the pressure distribution line and the cross section. First, the resulting forces of the pressure distribution can be computed, as shown in Eq. 7:

$$F_{\text{Horz}} = \int_{(A)} p\, \cos\phi\, dA$$
$$F_{\text{Vert}} = \int_{(A)} p\, \sin\phi\, dA \tag{7}$$

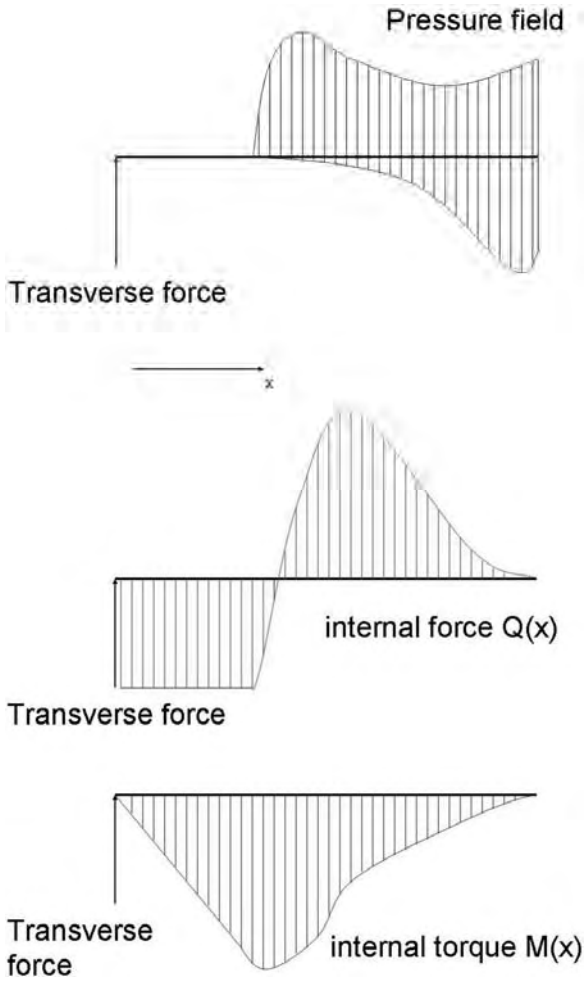

Fig. 4: *Internal force variables for the piston*

For the simulation tool the integral becomes a sum and the infinite area dA is enlarged to the macroscopic area A, which is the base area of one element of the lubricating film.

In a next step, the resulting forces act on the beam and influence the internal force. Therewith they cause internal torques according to the theory of bending beam.

An assumed pressure field and the transverse force, which are both acting on the piston, are shown in Fig. 4 in the top. The picture in the middle shows the internal force Q(x). The trend of the curve is influenced by the pressure field working on each cross section as it was shown in Fig. 3. The third picture shows the internal torque M(x). The slope of M(x) equals Q(x) or:

$$M(x) = \int Q(x)dx \tag{8}$$

Using the theory of bending beam ensures the equilibrium of forces and torques for the whole piston.

The working bending moment is proportional to the local curvature of the beam:

$$w''(x) = \frac{M(x)}{E\,I} \tag{9}$$

In Eq. 9, the variable $w''(x)$ is the second derivation of $w(x)$, which is the shifting of the piston axis. The variable $w'(x)$ represents the slope of the piston axis.

The boundary conditions are of high importance for the bending beam: in this case, there is a transverse force working on the piston's tip. The transverse forces on the piston's end as well as the torques on both ends have to be 0. The variables $w'(x)$ and $w(x)$ cannot be prescribed, because the piston can freely move in the cylinder.

2.3 Structure of the Simulation Model

Some other phenomena were taken into account: a simple model for mixed friction as well as a cavitation model is used. The model for mixed friction also considers local deformations in a simple manner. Moreover it is necessary to consider local deformations due to pressure peaks to get realistic results. All these models are kept rather simple to allow an easy implementation in the program.

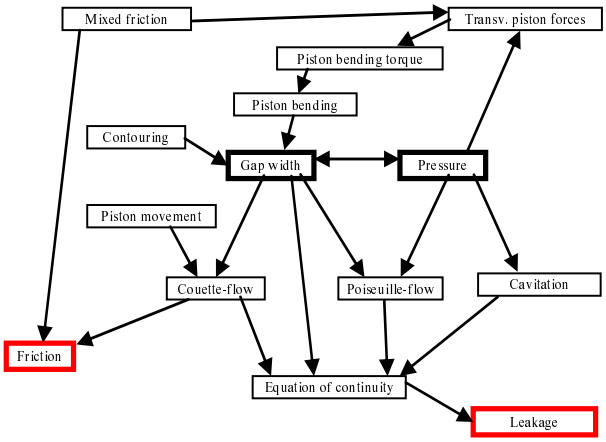

Fig. 5: *Structure of the simulation tool*

The conditions described above (short simulation time) caused restrictions in meshing and other phenomena: the temperature in the gap is assumed to be constant and therewith the oil viscosity. Figure 5 shows the inner structure of the simulation tool.

The simulation tool uses a constant time increment between two time steps. Keeping the time increment constant and having only first derivations to the time in the system of equations, the whole system can be described and solved with a single system matrix for each time step. Therewith the program has to be classified as a Finite-Element-Program rather than a numerical solver of a partial differential equation.

In contrast to all approaches described in chapter 1, the piston is simulated completely mass-free. This assumption is justifiable, because the piston movement in axial direction is prescribed by the kinematic of the machine, while the piston movement in radial direction (and therewith the speed and the acceleration in radial direction) are insignificant small.

With this assumption, the simulation program has two advantages over other simulation tools. Firstly, the coupling between a multiple body simulation and macros for the tribological equations is no longer necessary. Secondly, the very small forces for the piston's acceleration in radial direction are no longer taken into account. When using a multiple body simulation, the approach is that disequilibrium in the force or torque balance accelerates the piston. For an assumed piston movement from one side of the cylinder to the other and back with the same speed as the wobble plate, only very small accelerating forces are necessary (less than 1 N for common machine sizes at 2000 rpm). These small forces can be caused by numerical inaccuracies which results in unrealistic movement or oscillation of the piston inside the cylinder. To avoid these oscillations, the width of each time step must be reduced. The simulation therewith needs more computing power and time. Simulating the mass-free piston instead of using multiple body simulation reduces the simulation time to 15 minutes or less for a mesh width as it is shown below. Moreover the simulation program runs very stable and doesn't simulate unrealistic oscillations.

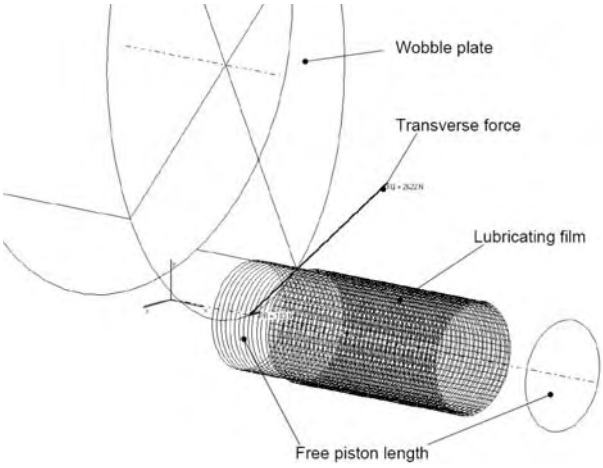

Fig. 6: *Meshed model for the lubricating film*

The program presented here works as a stand alone application, which was programmed using C++ and has a user-friendly interface and postprocessor. If MATLAB is present on the user's PC, it can be used as a fast solver for the system matrices.

The meshing of the lubricating film and of the piston is defined by a single parameter for the meshing width. Figure 6 shows an example for the meshing. Shown is the wobble plate, the meshing for the oil film and the meshing of the free piston length. The free piston length only has to be meshed at the piston's tip. The lower free end of the piston is completely free of internal forces and torques so that no equation has to be solved for this area. Moreover the applied transversal force is shown. The transversal force consists of the components F_Q and F_R, where F_Q is present because of the inclination of the wobble plate and F_R is caused by the (relatively low) friction between wobble plate and slipper. The simulation tool was first presented by Murrenhoff (2009).

3 Exemplary Simulation Results

The simulations performed and presented here use the piston geometry of an axial piston machine with a displacement of about 90 cc, a piston diameter of lmost 20 mm and a stroke of around 30 mm. All simulation results shown here were computed for pump mode. The angle of the wobble plate is 16° and the speed is 2000 rpm.

To compare the simulation results with test bench results, a single-piston test-bench was used. This test bench is based on the principle firstly presented by Renius (1974) and later improved by Breuer (2006), however for low speeds. The recently designed test-bench is suitable for high-speed tests and was firstly presented by Murrenhoff (2008). In order to get corresponding results, the simulation tool does not model the cylinder block of an original pump, but the inverse kinematics from this single-piston test-bench, as it is shown in Fig. 6. To make the simulation results comparable with these test bench results, the pressure in the piston chamber alternates between 50 bar (suction stroke) and 300 bar (pump stroke). The pressures are therewith higher than in the real machine.

A difference between the test bench and the real axial piston machine is the missing centrifugal force. However, the simulation results from the single-piston test-bench can be compared with the simulation results for the single-piston test-bench, on which the centrifugal force was switched off.

3.1 Build-up of the Lubricating Film

As assumed by Renius (1974) the local pressure in the piston-cylinder contact can reach higher values than the working pressure of the pump. The reason is that oil is drawn into a convergent gap by the Couette-flow. To fulfill the flow balance, the pressure in the convergent gap raises and the additional oil is transported away by the Poiseuille-flow. The same results are obtained with the simulation tool. Figures 7 and 8 show the local gap width and the local pressure for the same time step, both computed using the equations described above. The time step belongs to the pump stroke, the piston is moving into the cylinder. The wobble plate rotates counter-clockwise in both pictures.

The pistons middle axis is represented by the bold line in Fig. 7 and the local gap width h is represented by the thin mesh. When the piston middle axis moves downward, the local gap width at the lower side of the piston-cylinder-pair becomes smaller, while the gap widths at the upper side rise. The bending of the piston can be seen in the figure as well. The gap width and the shift of the middle axis are depicted raised by a factor of almost 1000.

Moreover a slight contouring of the piston can be seen in Fig. 7. First simulations showed that neglecting any contouring, even the contouring from running-in of ordinary brass or bronze-cylinders, results in unrealistic high friction forces. The reason is that a convergent gap for the hydrodynamic pressure build-up does not appear, when both, piston and cylinder, have an exact cylindrical shape. The contouring shown in Fig. 7 is rather small and is similar to the contour after a medium running-in phase of a conventional pump.

Due to the convergent gaps, the pressure locally increases. Figure 8 shows two local pressure peaks, a large one at the front end of the cylinder and a smaller one at the back end. Both pressure peaks are correctly positioned to bear the transverse force at the piston's tip. Therefore the force and torque equilibrium for the piston is fulfilled.

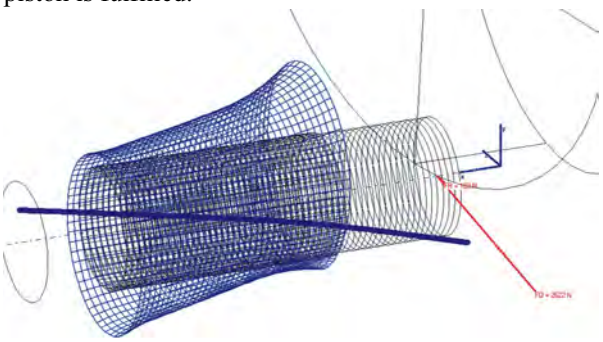

Fig. 7: *Local gap width and middle axis of piston*

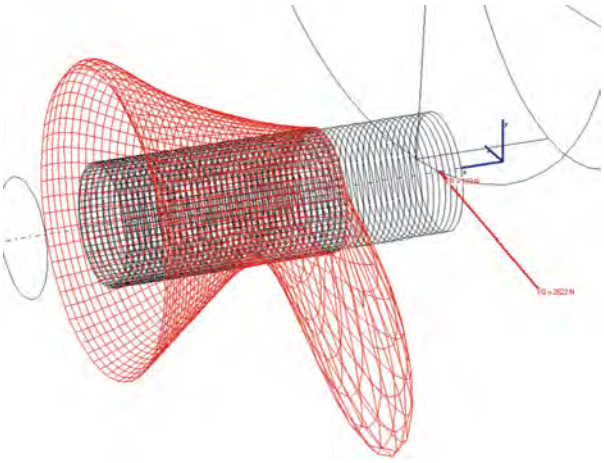

Fig. 8: *Local pressures*

3.2 Comparison with Test-Bench Results

To verify the simulation program, several simulations have been performed to compare them with test-bench results from the single-piston test-bench. As described above, a contouring has to be used for the cylinder to get realistic results.

The main results from the single-piston test-bench are the friction forces between piston and cylinder. The simulation tool was also used to compute the friction forces between piston and bushing. An exemplary result is shown in Fig. 9.

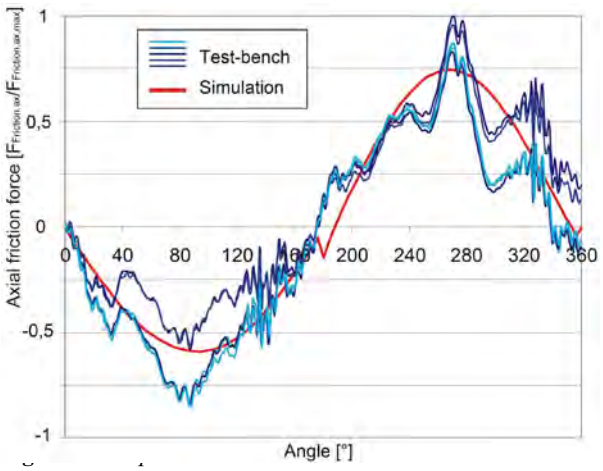

tion model

The mesh width for the simulation is as shown in Fig. 7 and Fig. 8. The simulation shows one rotation of the wobble plate for pump mode at 2000 rpm. The pressure is 50 bar in the suction stroke (0°-180°) and 300 bar in the pump stroke (180° to 360°). The pressure during the suction stroke is higher than in the real machine, to make the simulation results comparable with the test-bench, where lower pressures during the suction stroke are problematic. The oil viscosity for the simulation is around 40 mPas. The used oil on the test-bench has the same viscosity at 40 °C, at which the tests were performed. The angle of the wobble-plate is again 16° in the simulation and on the test-bench.

Because of measurement inaccuracies, 5 rotations of the test-bench are shown in the diagram. Oscillations from the measurement platform can be seen, which are not of interest here. It can be taken from the simulation program that the results of the simulation program coincide well with the test-bench results. The computed friction work due to axial piston movement is almost the same value for the simulation program and the test bench.

More comparisons between test-bench results and the simulation tool, for conventional cylinders and PVD-coated and contoured piston-cylinder-pairs, will be published in following papers.

4 Optimal Gap Width and Guidance Length

After having set up the simulation tool, the first optimizations were performed in order to find, which gap width and guidance length are optimal for a specified duty cycle. Since an axial piston pump should be optimized, the duty cycle is simply the constant rotational speed of 2000 rpm. The pressure changes from 50 to 300 bar, the angle of the wobble plate is 16°.

4.1 Benchmark for Optimization

An important question is, which benchmark should be selected for the optimization. The friction force between piston and cylinder in axial direction was already mentioned above. It can be used to compute the axial friction losses:

$$W_{ax} = \int F_{Friction,ax}\, ds \tag{10}$$

Moreover it is known that the piston rotates in the cylinder. The ratio between piston rotation and rotation of the wobble-plate is set to one. Therefore friction torque between piston and cylinder appears. The friction losses due to friction torque can be computed as follows:

$$W_{tng} = \int M_{Friction,tng}\, d\phi \tag{11}$$

A third component of losses are the leakage losses. To allow a comparison between friction and leakage losses, the leakage losses should be expressed as a single value as well:

$$W_{Leakage} = \int Q_{Leakage}(t)\Delta p(t)dt \tag{12}$$

The flow $Q_{Leakage}$ is the volume flow over the front end of the cylinder into the case of the pump while Δp is the pressure difference between pressure chamber and case.

The total losses can than be computed as:

$$W_{total} = W_{ax} + W_{tng} + W_{Leakage} \tag{13}$$

This value is used as benchmark for the following optimization process.

4.2 Gap Width and Guidance Length for the Piston-Cylinder-Contact

It is known, that higher gap widths reduce viscous friction but increase leakage. Moreover the appearance of mixed friction is more probable for a higher gap width, because the piston axis can tilt more. A similar correlation is valid for the length of guidance: if the guidance length is higher, the mixed friction is increased while the leakage is decreased and vice versa.

The gap width and guidance length should be optimized to reduce friction and leakage losses. Therefore simulations have been performed with variations of gap width and guidance length.

The results of this simulation are shown in Fig. 10. The curves are based on more than 250 simulation runs. The y-axis shows the computed total losses for one stroke. The different curves represent different gap widths, while the guidance length is shown on the x-axis.

The diagrams for axial friction losses and tangential friction losses are quite similar. An optimum guidance length can be found for each gap width. Usually the optimal guidance length is exactly so long that mixed friction is avoided. Further lengthening of the cylinder

has no advantage for the reduction of mixed friction but disadvantages because of the larger area where viscous friction appears. The optimal guidance length rises, when the gap width gets higher.

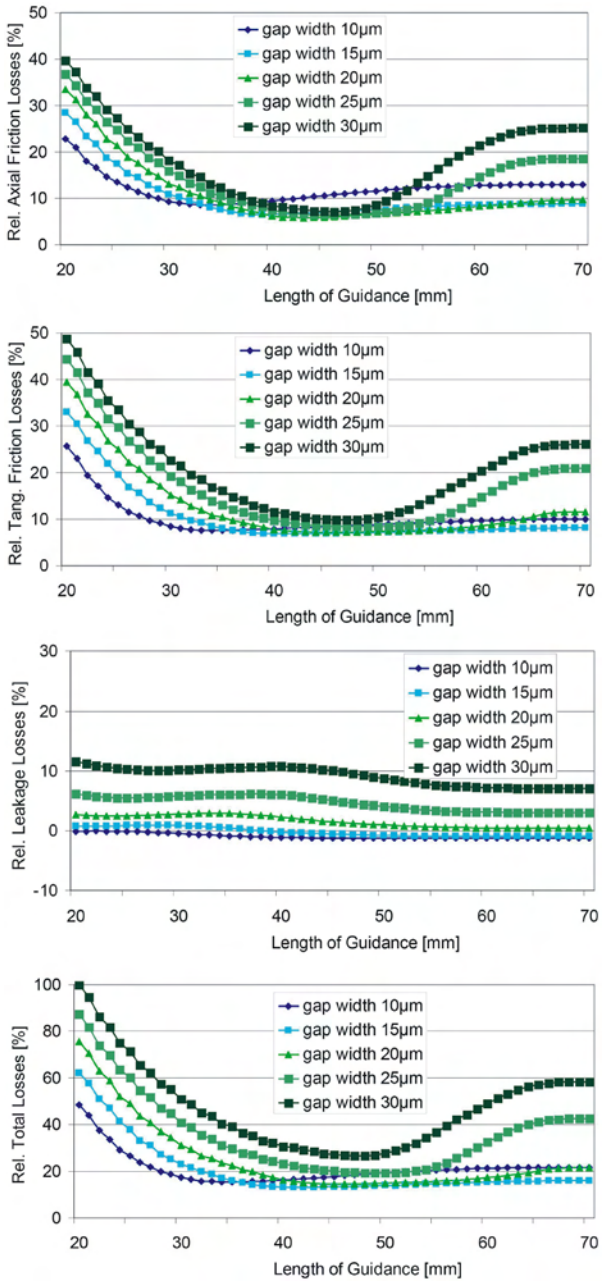

Fig. 10: *Variation of gap width and guidance length for the piston-cylinder-pair: axial friction, tangential friction, leakage losses and total losses*

The leakage losses are especially high for a short guidance length and high gap widths. The leakage losses can fall below zero for higher guidance length and small gap widths. The reason is that during the pump stroke oil is drawn into the cylinder against the high pressure in the piston chamber due to Couette-flow. Because of the high pressure difference during the pump stroke, this oil has a higher "value" in the integral of Eq. 12 than the oil which is drawn out during the suction stroke. This causes leakage losses smaller than 0, although the leakage flow still is positive and therewith the volumetric efficiency stays below 1.

The total losses are computed by simply adding all three losses according to Eq. 13. It can be seen from this diagram, that an optimum guidance length and gap width can be found for the investigated axial piston machine. The tangential and axial friction losses are dominating the curves in this diagram. Losses due to leakage only have an influence for higher gap widths. These high gap widths therefore become more and more unattractive in the diagram for total losses than they were in the two diagrams for friction losses.

For a speed of 1000 rpm the results are quite similar to the one for 2000 rpm, but the optimal ratio between guidance length and gap width is moved to a higher guidance length for a constant gap width. Because 2000 rpm is the rotational speed for which the pump has to be optimized, a gap width of 15 µm and a guidance length of 40 mm have been chosen for further optimization. Each pump or motor can be optimized in that way.

5 Results for Contoured Piston and Cylinder

Having found optimal values for gap width and guidance length, the contouring of piston and bushing can be varied. A contour can be applied to all 4 edges of cylinder and bushing. As the shape of the contour a circular arc with a tangential transition to the shaft has been chosen. This contouring seems to be superior to a spherical shape over the whole piston length, because it can better support the bending torque. For each contour a length and a radius is sufficient to define the geometry. The contouring of the whole piston-cylinder-pair is than defined by 8 parameters, as shown in Fig. 11.

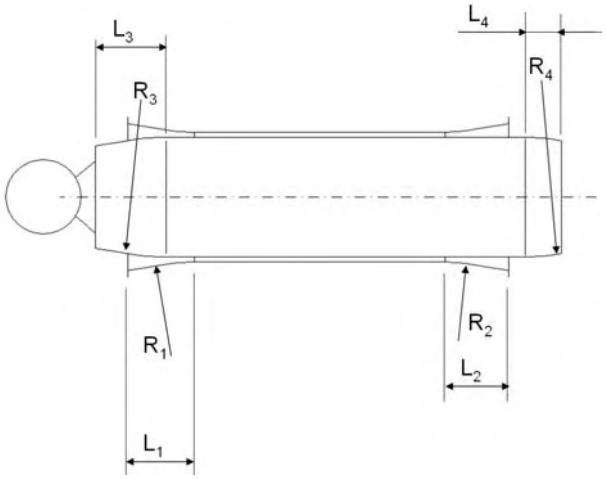

Fig. 11: *Contouring of piston and cylinder*

It is known from first tests that the front contour of the cylinder (R_1 and L_1) has the highest influence on friction forces and therewith friction losses as well as leakage losses. Therefore this contour was optimized first.

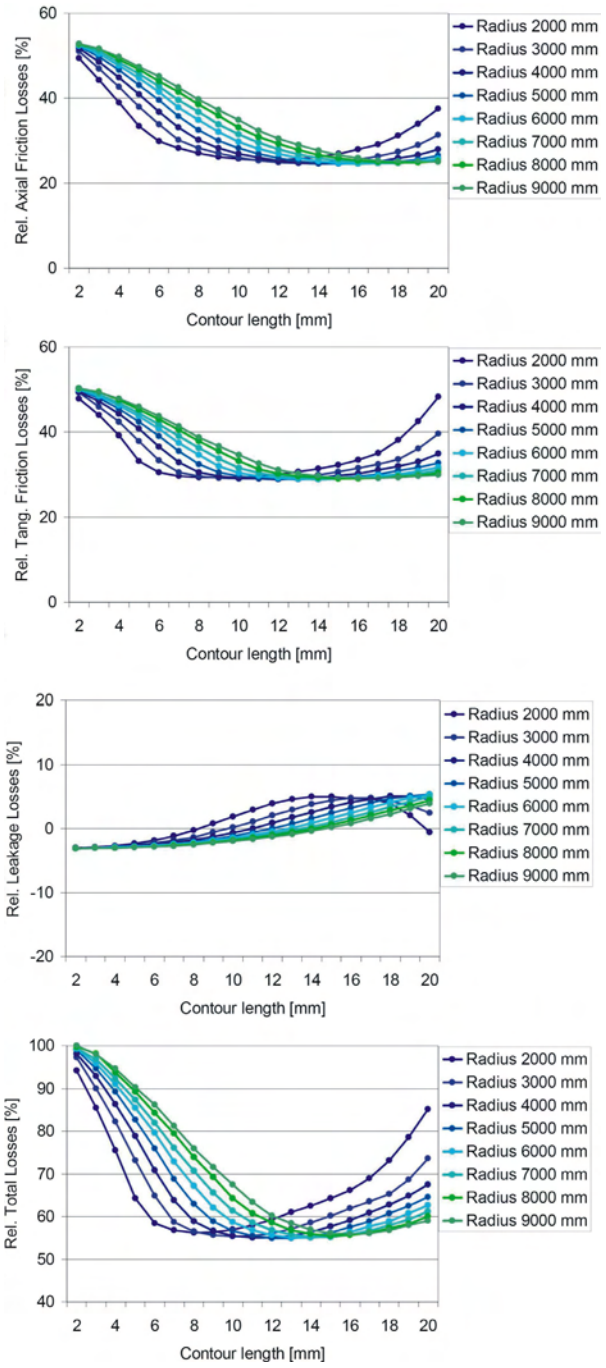

Fig. 12: *Variation of the front contour of the cylinder*

Figure 12 shows the results of the performed simulations. The diagram is based on more than 150 single simulations. The pump speed is again 2000 rpm. The contour length L_1 is shown on the x-axis, while the variation of the radius R_1 is represented by different curves. It has to be mentioned, that a low Radius and a high contour length means that a lot of material is "grinded" away from the cylinder. A radius of 2000 mm and a contour length of 20 mm means, that the cylinder's radius is increased by 100 µm on the edge. A contour length of 2 mm and a Radius of 9000 mm results in a contour which is widened by approximately 0.2 µm.

The scaling of the diagram is refined compared to Fig. 10. The simulation results show that an optimum (a minimum) for the total losses can be found for a contour length of 14 mm and a contour radius of 4000 mm. A lot of simulations in this area result in small total losses. Again, both friction losses dominate the leakage losses.

After having found good contours for the front of the cylinder, the back end of the piston and the back end of the cylinder were optimized. Theses contours seem to be the next important ones, because – together with the front of the cylinder – they support the piston and the high bending torque acting on it.

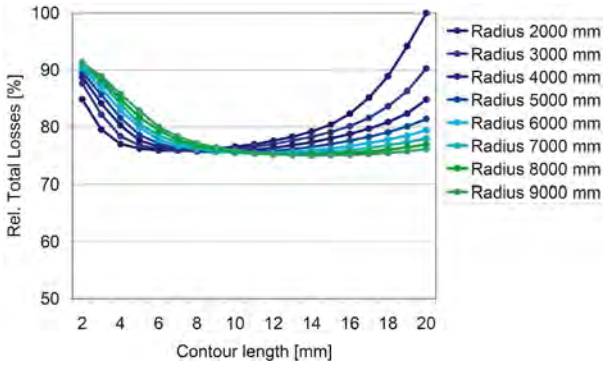

Fig. 13: *Variation of the back contour of the cylinder*

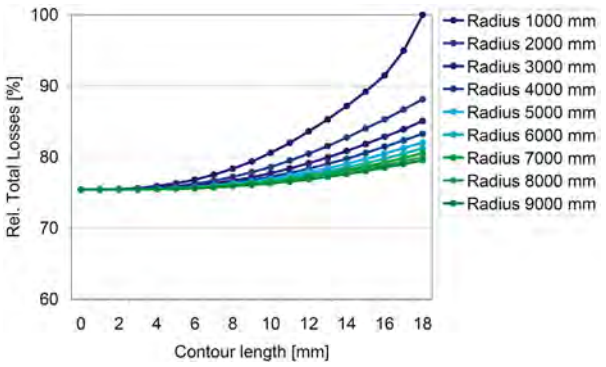

Fig. 14: *Variation of the back contour of the piston*

Figure 13 shows the variation of the back end of the cylinder, i. e. R_2 and L_2 from Fig. 11. Only the total losses are shown here. The diagram reminds of the diagram for total losses from Fig. 12. Again an optimum can be found for a specific contour. The simulations yield the result that the back end of the cylinder is optimized by a contour with a radius R_2 = 3000 mm and a length L_2 = 7 mm.

Figure 14 shows the simulation results for the variation of the back end of the piston, i.e. R_4 and L_4. From these results can be taken that a contour which is too long at the back end of the piston has a negative effect on the total losses of the piston. A small contour is helpful though, to reduce "scraping" of the sharp edge inside the cylinder. For further investigations a contour length of 7 mm and a radius of 5000 mm have been chosen.

As described for the front and back end of the cylinder and the back end of the piston, further simulations have been performed for the front end of the piston. The simulations for the front contour of the piston (R_3 and L_3) show that there is almost no influence on the total losses. The reason is that the front end of the piston only influences the build-up of the lubricating film,

when the piston is at its upper dead center, which corresponds to only 20-30% of the whole rotation of the wobble plate. But at this position the guidance length is rather high and the bending torque therewith low. The influence of this contour is therefore negligible.

6 Summary and Outlook

A simulation tool has been created to numerically compute the Reynolds equation for the lubricating film of the contoured piston-cylinder-contact of axial piston machines. This simulation tool enables the simulation of contoured pistons and cylinders.

With the help of this tool, simulations have been performed to find an optimal compromise between gap width and guidance length, which reduces the total losses of the piston-cylinder-pair during one stroke.

Following these findings more simulation runs were completed to find optimal contours for the edges of the cylinder and the bushing. The results of the simulation show that contouring of piston and cylinder can reduce the total losses significantly.

Within the next research phase contoured piston-cylinder-pairs will be machined and tested on the single-piston test-bench described above. Results will be discussed in further publications.

Acknowledgement

The project “Axial piston machines with PVD-coated components”, which is part of the Collaborative Research Centre (SFB) 442, is funded by the German Research Foundation. The authors would like to thank the German Research Foundation for its support.

Nomenclature

A	Area	[mm²]
A	Arbitrary term of Reynolds equation	[-]
b	Width of control volume	[mm]
E	Modulus of elasticity	[N/mm²]
F	Force	[N]
$F_{\text{Friction,ax}}$	Axial friction force between piston and cylinder	[N]
F_{Horz}	Horizontal force of a pressure field around a piston	[N]
F_{Vert}	Vertical force of a pressure field around a piston	[N]
h	Local gap width	[µm]
η	Dynamic oil viscosity	[mPas]
I	Geometric moment of inertia	[mm⁴]
l	Length of control volume	[mm]
φ	Angular position of a node	[°]
L	Length of Contouring	[mm]
$M(x)$	Internal bending moment	[Nm]
M	Bending moment	[Nm]
$M_{\text{Friction,tng}}$	Friction momentum between piston and cylinder	[Nm]
p	Local pressure	[bar]
$Q(x)$	Internal force	[N]
Q	Volume flow	[l/min]
Q_{Couette}	Coeutte-flow in gap	[mm³/s]
Q_{Leakage}	Leakage volume flow	[mm³/s]
Q_{Pois}	Poiseuille-flow in gap	[mm³/s]
R	Radius of contour	[mm]
s	Stroke of piston	[mm]
t	Time	[s]
U,V	Relative speed	[m/s]
W	Work, energy	[J, Nm]
W_{ax}	Losses due to axial friction forces	[J]
W_{Leakage}	Losses due to leakage	[J]
W_{tng}	Losses due to friction momentum	[J]
w	Position of bending line	[µm]
x,y,z	Coordinate system	[mm]

References

Van Bebber, D. 2003. *PVD-Schichten in Verdrängereinheiten zur Verschleiß- und Reibungsminimierung bei Betrieb mit synthetischen Estern*. Thesis, RWTH Aachen University.

Breuer, D. 2006. R*eibung am Arbeitskolben von Schrägscheibenmaschinen im Langsamlauf*. Thesis, RWTH Aachen University.

Deeken, M. and **Murrenhoff, H.** 2002. Advanced simulation of fluid of fluid power components using DSH*plus* and ADAMS. *Proceedings Bath workshop on power transmission and motion control, PTMC 2002*, Bath.

Ivantysyn, J. and **Ivantysynova, M.** 1993. *Hydraulische Pumpen und Motoren – Konstruktion und Berechnung*. Würzburg.

Kleist, A. 2002. *Berechnung von Dicht- und Lagerfugen in hydrostatischen Maschinen*. Thesis, RWTH Aachen University.

Lasaar, R. 2003. *Eine Untersuchung zur mikro- und makrogeometrischen Gestaltung der Kolben-/Zylinderbaugruppe von Schrägscheibenmaschinen*. VDI Fortschritt-Berichte. Reihe 1 No. 364. Düsseldorf: VDI. ISBN: 3-18-336401-8.

Liu, M. 2001. *Dynamisches Verhalten hydrostatischer Axialkolbengetriebe*. Diss., Bochum.

Manring, N. 1999. Friction forces within the cylinder bores of swash-plate type axial piston pumps and motors. *Journal of dynamic systems, measurement and control*, Vol. 121.

Murrenhoff, H., Piepenstock, U. and **Kohmäscher, T.** 2008. Analyzing losses in hydrostatic drives. *JFPS 2008*, Toyama, Japan.

Murrenhoff, H. and **Gels, S.** 2009. Improving efficiency of hydrostatic drives. *ICFP 2009*, Hangzhou, China.

Olems, L. 2001. *Ein Beitrag zur Bestimmung des Temperaturverhaltens der Kolben-Zylinder-Baugruppe von Axialkolbenmaschinen in Schrägscheibenbauweise*. VDI Fortschritt-Berichte. Reihe 1 No. 348. Düsseldorf: VDI. ISBN: 3-18-334801-2.

Patir, N. and **Cheng, H. S.** 1987. *Anaverage flow model for determining effects of three dimensional roughness on partial hydrodynamic lubrication*.

Renius, K. T. 1974. Untersuchungen zur Reibung zwischen Kolben- und Zylinder bei Schrägscheiben-Axialkolbenmaschinen. *VDI-Forschungsheft 561*, Düsseldorf, VDI-Verlag.

Sanchen, G. 2003. *Auslegung von Axialkolbenmaschinen in Schrägscheibenbauweise mit Hilfe der numerischen Simulation*. Thesis, RWTH Aachen University.

Scharf, S. and **Murrenhoff, H.** 2005. Measurement of friction forces between piston and bushing of an axial piston displacement unit. *International Journal of fluid power*.

Weichert, D. 1999. *Festigkeitslehre, Institut für allgemeine Mechanik.* RWTH Aachen, 4. Auflage.

Wieczorek, U. 2002. *Ein Simulationsmodell zur Beschreibung der Spaltströmung in Axialkolbenmaschinen der Schrägscheibenbauart*. VDI Fortschritt-Berichte. Reihe 7 No. 443. Düsseldorf: VDI. ISBN: 3-18-33307-4.

Stefan Gels
Born on December 15th, 1981, he received his degree in mechanical engineering (Dipl.-Ing.) at RWTH Aachen University, Germany in 2008. Since 2008 he has been member of the scientific staff at the Institute for Fluid Power Drives and Controls (IFAS) at RWTH Aachen University.

Hubertus Murrenhoff
Born on August 13th, 1953, he is director of the Institute for Fluid Power Drives and Controls (IFAS) and dean of faculty of mechanical engineering at RWTH Aachen University, Germany. Main research interests cover hydraulics and pneumatics including components, systems, controls, simulation programs and the applications of fluid power in mobile and stationary equipment.